RSC Advances

ROYAL SOCIETY OF CHEMISTRY

www.rsc.org/advances

Template-assisted synthesis of CdS nanocrystal arrays in chemically inhomogeneous pores by vapor-solid mechanism

Dmytro O. Grynko[a], Alexander N. Fedoryak[a], Oleg P. Dimitriev[a*]

Andrew Lin[b], Ramesh B. Laghumavarapu[b], Diana L. Huffaker[b]

Markus Kratzer[c], Yuri P. Piryatinski[d]

[a]V. Lashkaryov Institute of Semiconductor Physics, pr. Nauki 41, Kiev 03028, Ukraine

[b]University of California Los Angeles, 420 Westwood plaza, Los Angeles, CA, USA, 90095

[c] Institut für Physik, MontanUniversität Leoben, Franz-Josef-Straße 18, Leoben A-8700, Austria

[d] Institute of Semiconductor Physics, pr. Nauki 46, Kiev 03028, Ukraine

Keywords: CdS; nanocrystal; nanocavity; tetra-pod; multi-armed crystals; silicon nitride

ABSTRACT

An ordered array of CdS nanocrystals was synthesized by vapor-solid mechanism using a template of chemically inhomogeneous pores in the form of nanocavities in a thin silicon nitride layer on a SiO_2/Si wafer. The silicon oxide at the bottom of the Si_3N_4 cavities served for nucleation of the CdS crystals, whereas no affinity of CdS to silicon nitride was found. Tetra- and multi-pod morphology of the nanocrystals has been obtained. This morphology was attributed to a competition of nucleation rates and growth of different crystallographic planes at the Si_3N_4/SiO_2 and Si_3N_4/CdS interfaces, which is different from the polymorphism growth model.

*Corresponding author, e-mail address: dimitr@isp.kiev.ua

Introduction

CdS nanocrystals of different morphology and shape have attracted great attention in the recent years due to their potential application in various fields, such as optoelectronics, photovoltaics, sensors, catalysis, etc, and their relatively simple synthesis and large variety in attainable morphologies. For example, it has been demonstrated that single CdS nanowires (NWs) and nanobelts possess a lasing effect [1,2,3], ultralong CdS NWs can serve as optical waveguides [4], CdS crystals of NW morphology can be used for constructing of photovoltaic cells [5], etc. Tetrapod, star-shaped and hyper-branched semiconductor nanocrystals have attracted increasing interest due to promising applications in energy conversion devices [6], sensors [7], electronic gates [8], and their generally interesting optical properties [9], etc. The advantage of the tetrapod and hyper-branched morphology is an substantial increase in the surface-to-volume ratio of the nanocrystals and therefore it leads to higher contribution of processes which take place at the interface between nanocrystal and environment.

The design of specific templates to grow nanocrystals in ordered arrays is, however, a challenging problem. Attempts to design both "soft" and "hard" templates have been undertaken. Cavities in "soft" templates are in dynamic equilibrium and substances can diffuse into the cavity through the cavity well, while "hard" templates provide robust static pore channels where substances can enter into the pore channel through its opening only [10]. The use of "soft" templates like hexagonal liquid crystals [11,12], where both the symmetry and long-range order of the liquid crystals is preserved, as well as a 1-D inorganic coordination polymer ($KCd(SCN)_3$) [13] to grow bundles of CdS, CdSe, ZnS, etc., NWs has been reported. "Hard" templates, such as porous polymer membranes [14] and anodic aluminum oxides (AAO) [15] have been widely applied for the synthesis of semiconductor NWs and nanoparticles. The AAO template particularly takes a great advantage of arranging cylindrical pores of uniform diameter, which greatly benefits the fabrication of ordered NW arrays. Electrochemical and electroless deposition, chemical polymerization, sol-gel deposition, and

chemical vapor deposition are the major template synthetic strategies to obtain arrays of nanoparticles, NWs and nanotubules of metals, inorganic semiconductors, polymers in pores or channels.[16]

CdS nanocrystals have successfully been synthesized using templates of porous polymers [17], silica films [18], mesoporous silicate materials [19] and AAO membranes [20,21] by electrodeposition [22], gas-solid sulfurization reaction [23], and laser-induced [24], pressure-injection [25] . In contrast to the wet methods of synthesis, the "bottom-up" growth of ordered arrays of CdS nanocrystals in pores usually requires the presence of catalytic nucleation centers at the pore bottom, i.e., metallic seeds, which initiate the growth of nanocrystals through a vapor-liquid-solid (VLS) mechanism. The advantage of this method is that the shape and geometry of the nanocrystals can be controlled by the shape of the pores because during growth the liquid catalyst seeds fill the space available, thereby conforming to the pore geometry.[26] However, the preparation of such a template is rather difficult and expensive since it requires at least several technological steps, such as the preparation of the AAO membrane, barrier thinning, metal catalyst electrodeposition, etc.

Here, we describe a simple method of template-assisted synthesis of CdS nanocrystals free of catalyst, where the template pores themselves serve as nucleation centers for the nanocrystal growth. Such a synthesis is possible due to the design of chemically inhomogeneous pores using a combination of two materials, one of which has poor and the other high affinity with respect to CdS crystals grown through vapor-solid (VS) mechanism. This method also sheds more light on the combination of chemical and geometrical factors influencing the VS mechanism of nanocrystal growth.

Results and discussion

The synthesis procedure resulted in the formation of a CdS nanocrystal array wherein CdS nanocrystals only formed at the silicon nitride cavities and no crystal formation was observed on the flat Si_3N_4 surface (i.e., space between the holes and the outside of the patterned region) in SEM and AFM images of the samples (**Figure 1**). (Note that the crystals visible in between the cavities actually nucleate at the cavities and just point out parallel to the surface and do not grow on the Si_3N_4, as discussed below). Some crystallite-free cavities at the left edge of the sample can also be seen in Fig.1a which are believed to have survived due to incomplete etching of the Si_3N_4 surface during electron beam lithography, therefore still being silicon nitride terminated at the bottom. This behavior was always observed at the edges of the nanocavity array, whereas the cavities in the inner region of the array were always occupied by crystals (Fig. 1b). In Figs. 1c and 1d an AFM topography and the corresponding AFM phase image of a typical, single CdS tetrapod are shown. At the top right of the images in Figs. 1c and 1d a single arm that has been broken from the tetrapod is visible. The tetrapod has a height of 180 nm and a maximal lateral extension of roughly 400 nm, whereas individual arms have diameters between 120 and 170 nm. The length of the broken arm is about 200 nm. The AFM phase image in Fig. 1d just serves for better visualization of the facetted structure of the tetrapod.

The absence of CdS crystals on the flat Si_3N_4 surface was confirmed by fluorescence studies which showed no emission outside of the patterned region, whereas the patterned region with the cavity arrays which were arranged as regular squares (Fig.S1) emitted green light typical of luminescence of CdS [27] (**Figure 2a**).

The obtained results mean that the cavities terminated by silicon oxide at their bottom, on one hand, and silicon nitride at the side walls, on the other hand, possess significantly different affinity to CdS material. The growth of CdS crystals from gas phase occurs through condensation of the vapor on the surface which has a suitable affinity to the vapor

components and thus facilitates crystal nucleation. In our previous studies, it has been shown that CdS nanocrystals can grow by the VS mechanism on various surfaces of different chemical nature, such as quartz, indium-tin oxide, mica [28] and even carbon fibers [29], while no crystal growth was observed on the surface of high-purity graphite under the same synthesis conditions. An analogous difference has been found here with respect to silicon oxide and silicon nitride surfaces, respectively. A comparative growth experiment showed successful growth of CdS on a free silicon oxide surface while no growth was found on a pure silicon nitride surface under the same conditions (**Figure 3**). Although the driving mechanism of VS growth of CdS nanocrystals on different substrates at the early stage of nucleation is still under debate, some fine features can be distinguished. For example, it is known that CdS nanocrystals can be grown by van der Waals epitaxy on mica from a vapor transport process [30], whereas dipole-dipole and electrostatic interactions are probably responsible for adsorption on substrates possessing polar bonds, such as oxides. In this case CdS cation-anion molecules arrange themselves in a way that the proper local charge balance and the structural symmetry is maintained resulting in a nucleation center.[31] Apparently, the lack of strong polar bonds at the silicon nitride surface prevents a proper nucleation of CdS nanocrystals. We assume that the nucleation occurs through initial anchoring of Cd species from the CdS vapor to oxygen atoms of SiO_2 followed by joining of sulfur. The higher affinity of Cd to SiO_2 than to Si_3N_4 is due to a stronger polarity of the Si-O bonds compared to the Si-N bonds. The weak affinity of Cd to Si_3N_4 leads to diffusion of the Cd atoms over the surface until they meet atoms to which they have a higher affinity (i.e., oxygen of the SiO_2).

However, the chemical nature of the surfaces seems to be not the only factor that controls the crystal nucleation process. Such an assumption is consistent with the unusual morphology of the obtained nanocrystals in our case. Specifically, the crystals had a form of tetrapods or multi-armed nanorods, with a central trunk growing upward (roughly perpendicular to the surface) and additional arms extending from the central trunk along the

substrate surface (Figure 1d, **Figure 4a**). The changing thickness and morphology of the nanocrystals (Figure 4a) suggests that the growth of the final tetrapods or multi-armed nanorods occurs via two stages. The first step is a classical "bottom-up" growth through nucleation on the silicon oxide surface and extending of the crystal upward (normal to the surface) following the pore space (Figure 4a, crystal #1 which will be referred to further as a 'mother crystal'). Such a nucleation is characterized by a high mobility of the Cd and S species at the high growth temperature, where the newly arrived species do not condensate on the silicon nitride surface but tend to diffuse into the cavities which naturally slow down their motion due to steric hindrances. The second stage begins when the growing mother crystals start to stick out of the substrate surface. Then the Cd and S species diffusing over the silicon nitride surface collide with them and form new nucleation centers at the CdS/Si_3N_4 interface. The newly formed nucleation centers then give rise to growth of arms pointing away from the mother crystal axis. The growing arms can even suppress the growth of the mother crystal since they compete for the CdS material (see mother crystal 1 beneath the crystals 2 and 3 in Figure 4a, respectively). SEM, HRTEM (Figure 4) and FFT (**Figure 5**) images show that the crystal trunk and arms have the same hexagonal symmetry and measured interplanar distance of 6.67 Å which is attributed to crystallographic wurtzite structure oriented along the *c* axis (growth directions [0001]). As can be concluded from the EDX spectra of the central trunk (crystal #2 in Fig.4a) the ratio of Cd to S atoms in the different parts of the nanocrystal slightly varies, showing overall the excess of cadmium (**Figure 6**). In the lower part of the crystal, just above the substrate surface, the Cd to S ratio was determined to be 55:45. This ratio decreases in the middle and upper part of the crystal, being 52:48 and 51:49, respectively. Oversaturation of the lower part of the central trunk by cadmium confirms the above suggestion on crystal nucleation through initial anchoring of Cd species to surfaces to which they have high affinity, which gives rise to the growth of crystalline arms from the mother crystal.

The relatively narrow PL band of the tetra-/multi-pod nanocrystals (FWHM=32 nm, Fig. 2b) evidences that they have more perfect crystalline structure as compared to colloidal CdS nanoparticles whose PL band is broader and can possess additional features in the low-energy side of the spectrum.[32] At the same time, the PL band of the tetrapod crystals is asymmetric and broadened as compared with the PL band of CdS single crystals whose FWHM is 20 nm [27] (Fig. 2b), which reflects the presence of some disorder in the nanocrystalline sample. This disorder can be due to ionized defects in the nanocrystals which affect both width and shape of the PL band.[33] Indeed, emission of CdS crystals can be characterized as a superposition of two emission components located *ca.* at 504 and 515 nm which are assigned to the free exciton in CdS [34] and to the edge green emission due to recombination of a free electron and a hole bounded to the acceptor [35], respectively. The latter is related to the single-charged S^- ions which play the role of the acceptor [36] and contributes to the low-energy wing of the PL band. The S^- ions most probably are located at the nanocrystal surface and due to higher surface-to-volume ratio of tetrapod nanocrystals as compared to the bulk crystal they demonstrate a higher contribution to the spectrum of the nanocrystal array. Deflection from the crystal stoichiometry due to excess of cadmium as discussed above can also contribute to the broadening and asymmetry of the PL band.

The obtained results indicate that spatial inhomogeneity (cavities) influences the crystal growth and morphology significantly. It is known that at high temperatures the NW crystal growth by VS mechanism proceeds via a self-organization process, where a certain crystalline face attains some preference and plays the role of a nucleation seed to facilitate further crystal growth.[37,38] The tetrapod morphology of CdS nanocrystals is normally explained by the polymorphism model of growth [39,40] which implies the presence of a cubic zinc blende structure as a nucleation seed for such a growth [31]. Both zinc blende and wurtzite crystalline phases have one set of facets in common. The {111} facets of zinc blende structure are atomically identical to the ±(0001) facets of the wurtzite structure. Therefore, the wurtzite

arms can grow out of the {111} facets of the zinc blende core. The synthesis temperature is of great importance for such a process. It has been reported that multi-armed CdS nanocrystals can grow at low (~120 ^{0}C) temperatures, whereas at high temperatures only straight nanorods are produced. [41] The two different phases coexist in certain temperature regimes (~120 to 180 ^{0}C) [42] Different growth rates between the crystallographic surfaces can result in bi-, tri-, or tetrapods from zinc blende-phased seeds. Tetrapods are formed at the mildest growth condition at 120 ^{0}C, where the formation of the four arms proceeds evenly on the four different {111} surfaces of the CdS zinc blende core to form (001) faces of the wurtzite-phased arms. Bi- or tripods are obtained when the growth becomes faster at higher temperature (~180 ^{0}C).

However, the more complex morphology observed in our case in the form of multi-armed crystals as well as asymmetric displacement of the arms at irregular angles in the tetrapod nanocrystals (Figure 4a) indicates that the arms do not necessary match the crystal structure of the trunk, which makes the above model inapplicable. Moreover, the synthesis temperature of the tetrapod crystals in our case (~600 ^{0}C) was much higher than the above-mentioned temperature for the synthesis of multi-armed crystals described by polymorphism model. As an alternative mechanism, one should expect that nucleation is favorable on some specific surface defects or interface inhomogeneity [27], which can result in a more rapid formation of a nanocrystal arm under the vapor supersaturation conditions. The CdS/Si_3N_4 interface seems to play the role of such a spatial inhomogeneity which gives rise to the preferred growth of CdS arms from the mother trunk through a self-catalytic process.

Experimental Section

Template preparation: Prefabricated wafers of semiconductor monocrystalline silicon with orientation <100> were used as substrates for growth of CdS. The wafers were coated with a layer of silicon nitride with a thickness of about 14 nm (according to

ellipsometric investigations). Holes of 80 nm diameter were made by electron beam lithography and Oxford RIE etcher. The distance between the holes varied from 200 to 600 nm for different samples (supporting information, Fig. S1). As the substrates were exposed to air, a thin layer of native silicon oxide formed at the Si bottom of the holes. Before the growth of CdS nanocrystals in the holes, the thickness of the silicon oxide layer in the holes was reduced by etching in a solution of hydrofluoric acid. It should be noted that the samples have not been protected against ambient atmosphere upon transfer to the deposition chamber, therefore, the silicon oxide layer persisted even on the etched samples as well.

Nanocrystal synthesis: The synthesis of the CdS nanocrystals was performed by close space sublimation technique in a vessel with hot walls onto the heated substrates prepared as described above. CdS and S powders served as precursors. The typical temperature of the CdS evaporation was 745 ^{0}C and the substrates were heated to 515- 635 ^{0}C. The growth time was about 5 minutes. The quasi-closed vessel was made of quartz and graphite. Preliminary pumping of the vessel was performed by cryosorption techniques to reach a pressure of 10^{-6} mm Hg.

Microscopy studies: Samples have been studied by scanning electron microscopy (SEM) using JEOL JSM35, JXA-8200. Detailed structural analysis was done by transmission electron microscopy (TEM) using a FEI Titan 300kV S/TEM. The TEM sample was prepared by mechanical transfer of the CdS nanocrystals onto a standard 3 mm copper TEM grid. To study the crystal structures in the CdS nanocrystals, fast fourier transform (FFT) was performed in different regions of the HRTEM image. AFM studies were carried out under ambient conditions using an MFP 3D system from Asylum Research. The AFM was operated in intermittent contact mode (Tapping mode) using ProbeMax carbon nanotube atomic force microscope probes with a resonance frequency of 230 kHz.

Fluorescence studies: Fluorescence images of the samples have been obtained by using fluorescence microscopy. In these studies, a 380 nm diode laser was used as an excitation source to illuminate the sample and a microscope XY-B2 equipped with a long pass filter with the edge at ~450 nm was used to cut blue and UV light scattered from the sample. Photoluminescence (PL) spectra were measured using a nitrogen laser (λ_e = 337 nm) as the excitation source, whose pulse width was 9 ns, the power of pulse emission 5 kW and the pulse repetition rate 70 Hz. Emission was registered through an MDR-12 grate monochromator equipped with a photomultiplier tube counter, an amplitude discriminator and a coincidence circuit. The final spectra were corrected for the spectral sensitivity of the registering system.

Conclusion

In summary, we have demonstrated the successful growth of an ordered array of CdS nanocrystals via VS mechanism using a template of chemically inhomogeneous cavities. The tetra- and multi-pod morphology of the obtained crystals was explained by competition of nucleation rates and growth of different crystallographic planes at the Si_3N_4/SiO_2 and Si_3N_4/CdS interfaces. The demonstrated method opens up a new way for preparation of ordered arrays of nanocrystals for specific applications.

Acknowledgements

This publication is based on work supported by Award No. UKE2-7035-KV-11 of the U.S. Civilian Research & Development Foundation (CRDF). The work was also supported by the Ministry of Education and Science of Ukraine. Support by the Austrian Academic Exchange Service (ÖAD) in the framework of the bilateral project UA 05/2013 is acknowledged.

References

[1] X.F. Duan, Y. Huang, R. Agarwal, C.M. Lieber, *Nature* **2003**, 421, 241.

[2] Y.K. Liu, J.A. Zapien, C.Y. Geng, Y.Y. Shan, C.S. Lee, Y. Lifshitz, S.T. Lee, *Appl. Phys. Lett.* **2004**, 85, 3241.

[3] A.L. Pan, R.B. Liu, B.S. Zou, *Appl. Phys. Lett.* **2006**, 88, 173102.

[4] G.Z. Dai, Q. Wan, C.J. Zhou, M. Yan, Q.G. Zhang, B.S. Zou, *Chem. Phys. Lett.* **2010**, 497, 85.

[5] a) J. Tang, Z. Huo, S. Brittman, H. Gao, P. Yang, *Nature Nanotechnol*. **2011**, 6, 568; b) D.O. Grynko, O.M. Fedoryak, P.S. Smertenko, N.A. Ogurtsov, A.A. Pud, Yu.V. Noskov, O.P. Dimitriev, *J. Nanosci. Nanotechnol.*, **2015,** 15, 752.

[6] a) R. Buonsanti, E. Carlino, C. Giannini, D. Altamura, L. De Marco, R. Giannuzzi, M. Manca, G. Gigli, P. D. Cozzoli, *J. Am. Chem. Soc.* **2011,** 133, 19216; b) H. Zhong, Y. Zhou, Y. Yang, C. Yang, Y. Li, *J. Phys. Chem. C* **2007**, 111, 6538.

[7] K . Wang, X.M. Qian, L. Zhang, Y.G. Li, H.B. Liu, *ACS Appl. Mater. Interfaces* **2013,** 5, 5825.

[8] a) N. Chen, S. Chen, C. Ouyang, Y. Yu, T.F. Liu, Y.J. Li, H.B. Liu, Y.L. Li, *NPG Asia Mater.* **2013,** 5, e59; b) W. Fu, S. Qin, L. Liu, T.-H. Kim, S. Hellstrom, W. Wang, W. Liang, X. Bai, A.-P. Li, E. Wang, *Nano Lett.* **2011**, 11, 1913.

[9] a) A. A. Lutich, C. Mauser, E. Da Como, J. Huang, A. Vaneski, D. V. Talapin, A. L. Rogach, J. Feldmann, *Nano Lett.* **2010**, 10, 4646; b) D. V. Talapin, J. H. Nelson, E. V. Shevchenko, S. Aloni, B. Sadtler, A. P. Alivisatos, *Nano Lett.* **2007**, 7, 2951.

[10] C.J. Murphy, N.R. Jana, *Adv. Mater.* **2002,** 14, 80.

[11] P.V. Braun, P. Osenar, S.I. Stupp, *Nature* **1996**, 380, 325.

[12] X. Jiang, Y. Xie, J. Lu, L. Zhu, W. He, Y. Qian, *Chem. Mater.* **2001**, 13, 1213.

[13] X. Zhang, Y. Xie, Q. Zhao, Y. Tian, *New J. Chem*. **2003**, 27, 827.

[14] C. Schönenberger, B. M. I. van der Zande**,** L.G.J. Fokkink, M. Henny, C. Schmid, M. Krüger, A. Bachtold, R. Huber, H. Birk, U. Staufer, *J. Phys. Chem. B*, 1997, 101, 5497.

[15] J. C. Hulteen, C.R. Martin, *J. Mater. Chem.* **1997**, 7, 1075.

[16] A. Huczko, *Appl. Phys. A* **2000,**70, 365.

[17] B.J.S. Johnson, J.H. Wolf, A.S. Zalusky, M.A. Hillmyer, *Chem. Mater.* **2004,** 16, 2909.

[18] S. Besson, T. Gacoin, C. Jacquiod, C. Ricolleau, J.P. Boilot, *Mater. Res. Soc. Symposium – Proc.* **2002,** 707, 119.

[19] E.A. Turner, Y. Huang, J.F. Corrigan, *Europ. J. Inorg. Chemistry*, **2005,** 22, 4465.

[20] D. Xu, Y. Xu, D. Chen, G. Guo, L. Gui, Y. Tang, *Adv. Mater.* **2000,** 12, 520.

[21] D. Xu, Y. Xu, D. Chen, G. Guo, L. Gui, Y. Tang, *Chem. Phys. Lett.* **2000,** 325, 340.

[22] A. Aguilera, V. Jayaraman, S. Sanagapalli, R. Suresh Singh, V. Jayaraman, K. Sampson, V.P. Singh, *Sol. Energy Mater. Sol. Cells* **2006,** 90, 713.

[23] Q. Wang, G. Chen, C. Zhou, R. Jin, L. Wang, *J. Alloys and Compounds* **2010,** 503, 485.

[24] B. Capoen, A. Chahadih, H. El Hamzaoui, O. Cristini, M. Bouazaoui, *Nanoscale Res. Lett.* **2013**, 8, 266.

[25] N. Petkov, J. Xu, M.A. Morris, J.D. Holmes, *J. Phys. Chem. C* **2008,** 112, 7345.

[26] O. Ergen, D.J. Ruebusch, H. Fang, A.A. Rathore, R. Kapadia, Z. Fan, K. Takei, A. Jamshidi, M. Wu, A. Javey, *J. Am. Chem. Soc.* **2010,** 132, 13972.

[27] A.F. Syngaevsky, Yu.P. Piryatinski, D.O. Grynko, O.P. Dimitriev, *Appl. Physics A* **2011,** 104, 493.

[28] D.A. Grynko, A.N. Fedoryak, O.P. Dimitriev, A. Lin, R.B. Laghumavarapu, D.L. Huffaker, *Surf. Coatings Technol.* **2013,** 230**,** 234.

[29] P.S. Smertenko, D.A.; Grynko, N.M. Osipyonok, O.P. Dimitriev, A.A. Pud, *Phys. Stat. Solidi A,* **2013,** 210**,** 1851.

[30] M.I.B. Utama, Z. Peng, R. Chen, B. Peng, X.L. Xu, Y.J. Dong, L.M. Wong, S.J. Wang, H.D. Sun, Q.H. Xiong, *Nano Letters* **2011,** 11, 3051.

[31] S. Kar, S. Chaudhuri, *Synth. React. Inorg. M.* **2006,** 36, 289.

[32] N.M. Osipyonok, A.F. Singaevsky, Yu.V. Noskov, Yu.P. Piryatinski, P.S. Smertenko, O.P. Dimitriev, A.A. Pud, *Mater. Sci. Engineering B* **2008,** 147, 254.

[33] A. P. Levanyuk, V. V. Osipov, *Sov. Phys. Usp.* **1981,** 24, 187.

[34] N.A. Vlasenko, Z.L. Denisova, *J. Lumin.* **1984**, 31, 412.

[35] L.S. Pedrotti, D.C. Reynolds, *Phys. Rev.* **1961,** 120, 1664.

[36] N.A. Vlasenko, Z.L. Denisova, N.I. Vitrikhovsky, V.D. Pavlenko, *Opt. Spectrosc.* **1966,** 21, 466.

[37] L. Chen, X. Fu, J. Lai, J. Sun, Z. Ying, J. Wu, N. Xu, *J. Electron. Mater.* **2012**, 41, 1941.

[38] J.G. Lu, P. Chang, Z. Fan, *Mater. Sci. Engineering R* **2006,** 52, 49.

[39] X.L. Fu, Z.J. Peng, D. Li, L. Zhang, J.H. Xiao, J.Y. Li, Z.Y. Fang, *Nanotechnology* **2011**, 22, 175601.

[40] S. Kudera, L. Carbone, L. Manna, W.J. Parak, in *Semiconductor Nanocrystal Quantum Dots. Synthesis, Assembly, Spectroscopy and Applications* (Eds.: A. Rogach) Springer-Verlag, Wien, Austria **2008**, pp.1-34.

[41] Y. Jun, S. M. Lee, N. J. Kang, J. Cheon, *J. Am. Chem. Soc*. **2001**, 123, 5150.

[42] O. Zelaya-Angel, J. J. Alvaradi-Gol, R. Lozada-Morales, H. Vargas, A. Ferreira da Silva, *Appl. Phys. Lett*. **1994**, 64, 291.

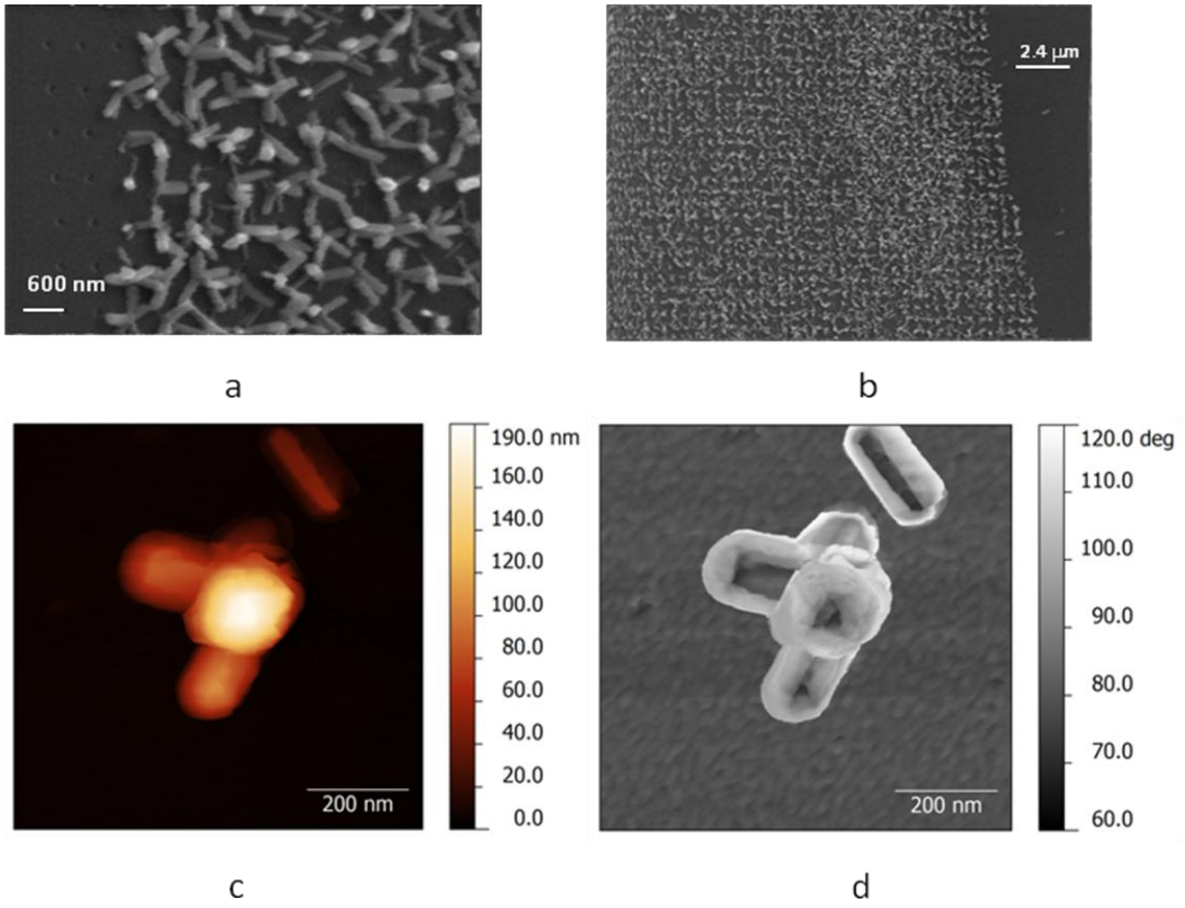

Figure 1. (a,b) SEM images of tetrapod nanocrystal arrays grown in cavities of the silicon nitride surface; the cavities regularly cover the whole Si_3N_4 surface, however, some holes in (a) survived the deposition procedure due to incomplete etching. AFM of (c) topography and (d) phase image of a single tetrapod CdS crystal; one arm has been broken.

a

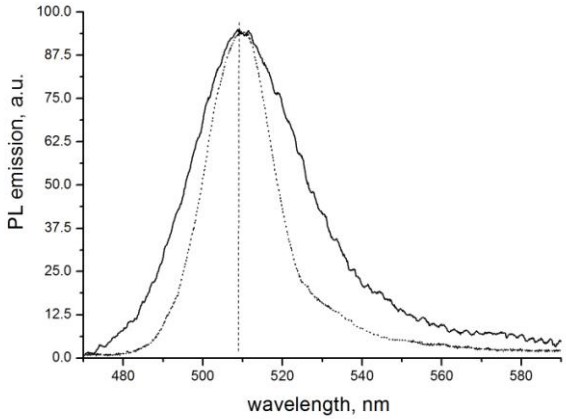

b

Figure 2. (a) Fluorescence microscopy image (the shape of the emitted region conforms that of a separate cavity array of the patterned substrate (Fig.S1)) and (b) PL emission spectrum of the array of CdS tetrapod nanocrystals (solid curve) compared with PL emission of the single CdS crystal (dotted curve, adapted from ref. [27]).

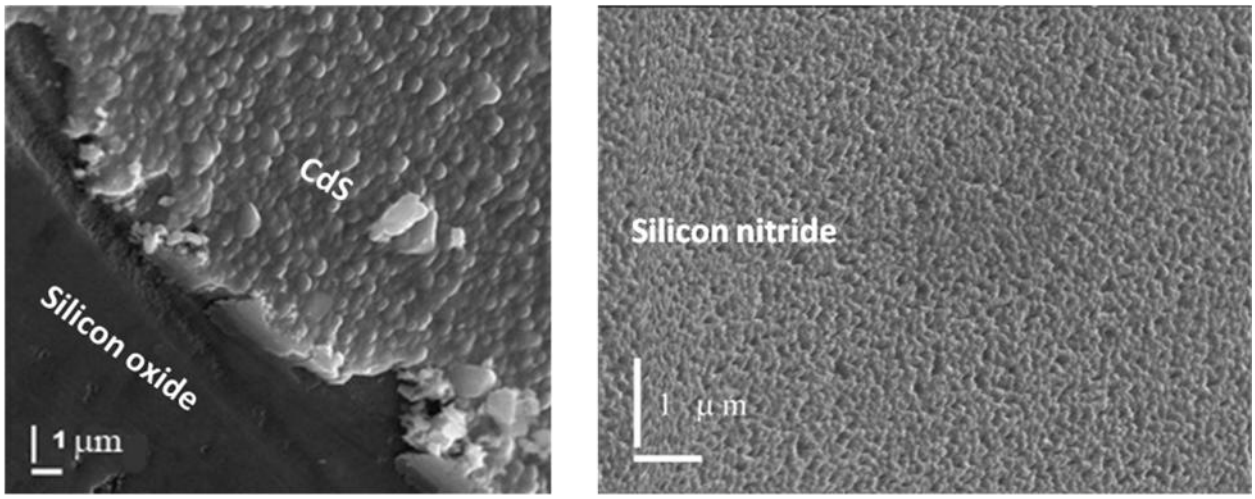

Figure 3. SEM images of (a) silicon oxide and (b) silicon nitride surfaces after the CdS deposition process performed under the same conditions. CdS layer is seen only in (a) and its edge is shown for clarity.

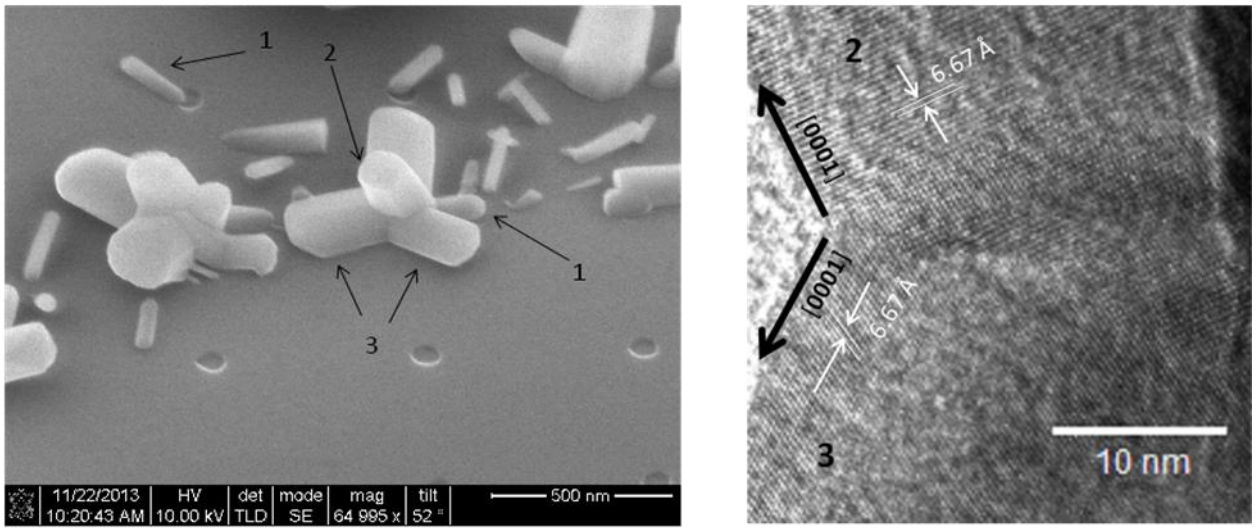

a b

Figure 4. (a) SEM and (b) HRTEM images of tetrapod nanocrystals. Arrows in (b) show the direction of growth of the central trunk (crystal #2) and the arm (crystal #3), respectively.

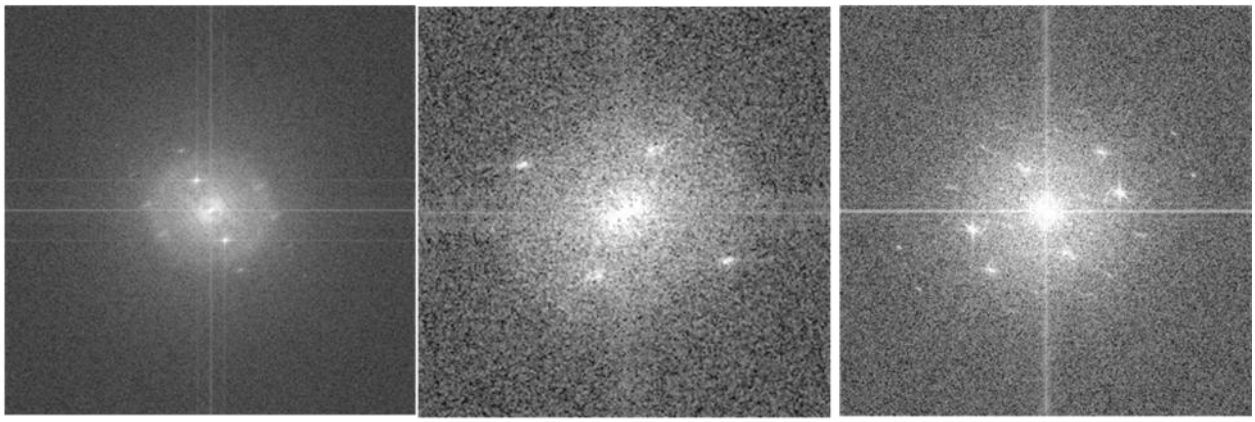

a b c

Figure 5. FFT images of (a) central vertical trunk, (b) horizontal arm and (c) intermediate region at the cross of the trunk and the arm nanocrystals.

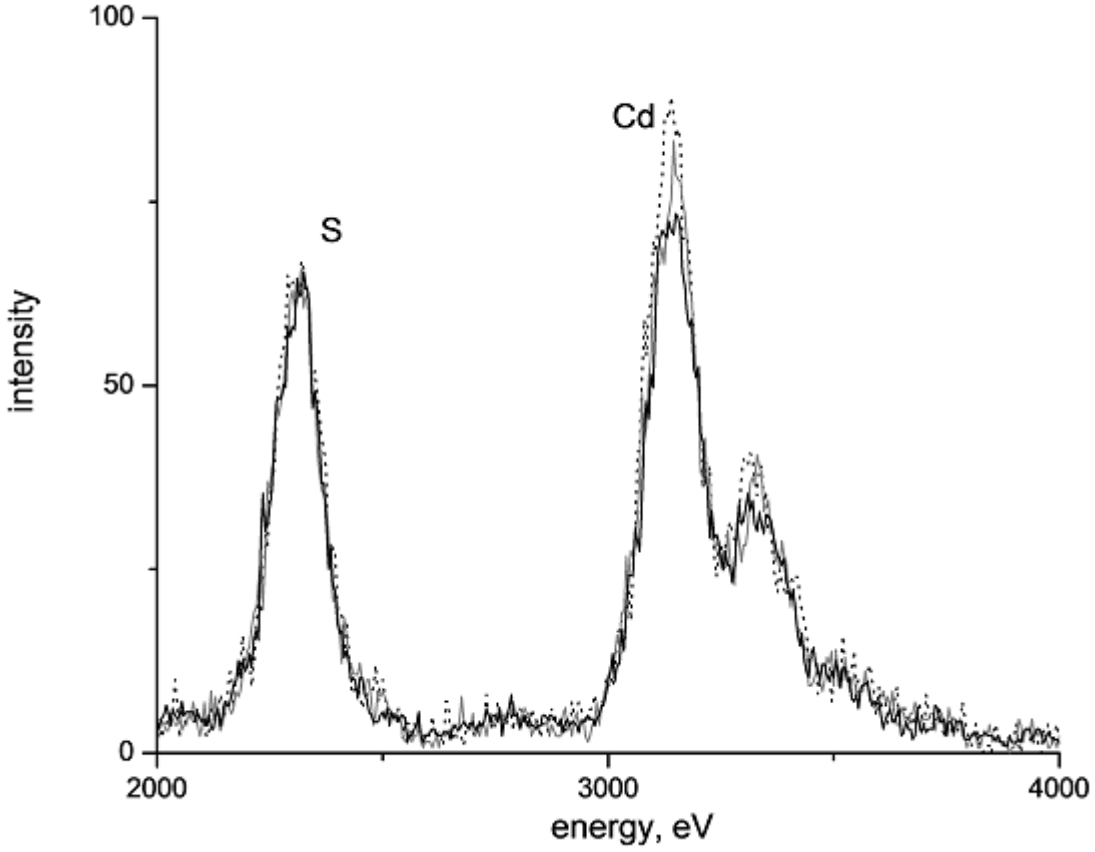

Figure 6. EDX spectra of the upper (solid black curve), middle (grey solid curve) and lower (dotted curve) part of the central trunk (crystal #2) of the CdS tetrapod.